One can note that, in general, the observed displacements in $Ni_{17}S_{18}$ relative to the ideal positions in the reference NiAs subcell are rather small; this contrasts with the larger displacements observed, for instance, for the superstructure in $Fe_{1-x}S$. Such small displacements further explain the weaker superstructure reflections of $Ni_{17}S_{18}$ and the greater difficulties encountered for their experimental recording (the need of monochromatic radiation is more common for diffuse scattering than for Bragg reflections).

Finally, in the ideal subcell each Ni atom would be in the centre of an octahedron with six Ni–S distances equal to 2·39 Å. In $Ni_{17}S_{18}$ the average Ni–S distances are in the same range (2·37 to 2·40 Å); the smallest and largest individual distances are respectively 2·30 and 2·48 Å. These last distances both occur in the surrounding of the strongly displaced Ni(4) atom, while the distances with the vacant Ni site are normally relaxed (2·44 Å on average).

6. Conclusion

The structure of the first vacancy-ordered compound described in the $Ni_{1-x}S$ system can be solved using a microtwinned model which respects at the same time the observed extinction condition and the fundamental NiAs-type stacking of nickel and sulphur atoms. The validity of the model is established first by the satisfactory value of the R factor obtained in the refinement and also by the analysis of the stacking fault responsible for the microtwinning. In these conditions the complete structure is described at the same time in its ordered aspects as well as in its disordered ones.

References

BARTHELEMY, E., CHAVANT, C., COLLIN, G. & GOROCHOV, O. (1976). *J. Phys (Paris) Colloq.* **4**, 17–22.

COWLEY, J. M. (1976*a*). *Acta Cryst.* A**32**, 83–87.

COWLEY, J. M. (1976*b*). *Acta Cryst.* A**32**, 88–91.

COWLEY, J. M. & AU, A. Y. (1978). *Acta Cryst.* A**34**, 738–743.

FLEET, M. E. (1971). *Acta Cryst.* B**27**, 1864–1867.

GUINIER, A. (1956). *Théorie et Technique de la Radiocristallographie.* Paris: Dunod.

JAGODZINSKI, H. (1949*a*). *Acta Cryst.* **2**, 201–207.

JAGODZINSKI, H. (1949*b*). *Acta Cryst.* **2**, 208–214.

JAGODZINSKI, H. (1949*c*). *Acta Cryst.* **2**, 298–304.

JAGODZINSKI, H. (1954). *Acta Cryst.* **7**, 17–25.

KAKINOKI, J. (1967). *Acta Cryst.* **23**, 875–885.

KAKINOKI, J. & KOMURA, Y. (1952). *J. Phys. Soc. Jpn*, **7**, 30–36.

KAKINOKI, J. & KOMURA, Y. (1954*a*). *J. Phys. Soc. Jpn*, **9**, 165–176.

KAKINOKI, J. & KOMURA, Y. (1954*b*). *J. Phys. Soc. Jpn*, **9**, 177–183.

KELLER-BESREST, F., COLLIN, G. & COMÈS, R. (1983). *Acta Cryst.* B**39**, 296–303.

NAKANO, A., TOKONAMI, M. & MORIMOTO, N. (1979). *Acta Cryst.* B**35**, 722–724.

Acta Cryst. (1982). B**38**, 296–303

Structure and Planar Faults in the Defective NiAs-Type Compound 3*c* Fe_7S_8

BY F. KELLER-BESREST AND G. COLLIN

Laboratoire associé au CNRS n° 200, 4, avenue de l'Observatoire, 75006 Paris, France

AND R. COMÈS

Laboratoire de Physique des Solides, Associé au CNRS n° 2, Bâtiment 510, Université Paris-Sud, 91405 Orsay, France

(*Received* 22 *February* 1980; *accepted* 22 *November* 1982)

Abstract

The structure of 3*c*-type iron sulphide, Fe_7S_8, grown by vapour transport was re-examined; $a = 6·866$ (1), $c = 17·088$ (2) Å. The R factor obtained with the microtwinned model is 4·25% for 573 reflections. The incomplete ordering of the vacancies is explained by the occurrence of about 20% 4*c* sequences in the overall 3*c* lattice. The quantitative analysis of the diffuse streaks using Cowley's theory allows the interpretation of the microtwinning mechanism as a translation vector $\pm$ (**a** – **b**)/6 in the superstructure cell. The calculated fault rate is equal to 0·03.

1. Introduction

Numerous structural studies have already been devoted to the various NiAs-type phases encountered in the $Fe_{1-x}S$ system. Many of them were performed on natural crystals and a great number of superstructures of the main NiAs-type lattice have been found. In

0108-7681/83/030296-08$01.50 © 1983 International Union of Crystallography

contrast, laboratory-grown crystals correspond only to some of these vacancy-ordered compounds and are generally more disordered than the natural ones. In one case only has it been possible to obtain a laboratory-grown compound, for the lower iron content of the NiAs-type homogeneity range Fe_7S_8 (pyrrhotite) which is known under two modifications:

a form found in nature which exhibits a slight monoclinic deformation ($\gamma = 89{\cdot}63°$). It is commonly designated at the $2a$–$2a$–$4c$ type (a and c are lattice constants of the NiAs-type subcell). Its structure was first studied by Bertaut (1953) and more recently by Mukherjee (1969) and by Tokonami, Nishigushi & Morimoto (1972);

the second form is strictly hexagonal with a superlattice $2a$–$2a$–$3c$ and only obtained by synthesis. Initial structural analysis was proposed by Fleet (1971) and more recently by Nakano, Tokonami & Morimoto (1979); both papers describe this form as microtwinned with strictly ordered vacancies.

Electron microscopy of the $4c$ monoclinic-type pyrrhotite was also performed on natural crystals by Van Landuyt & Amelinckx (1972) and by Nakazawa, Morimoto & Watanabe (1975). These authors have interpreted their lattice imaging in terms of defects such as antiphase boundaries, stacking faults and twinning (due to the monoclinic deformation) associated with changes only occurring in the vacancy ordering and without modification of the average NiAs lattice.

Fe_7S_8 seems to be the only compound in the series of NiAs-type defective structures for which a 'polymorphism' of superstructures is observed. The purpose of the present paper is to describe the relationships between the two existing phases and the microtwinning mechanism as already done for $Ni_{17}S_{18}$ by Collin, Chavant & Comès (1983), hereafter referred to as paper I.

We observe in Fe_7S_8 the same type of planar defect as already found for $Ni_{17}S_{18}$. The analysis of the faults performed using the theory developed by Cowley allows a quantitative treatment of the planar defects with a limited number of parameters. The papers by Cowley (1976*a*, *b*) and Cowley & Au (1978) will be referred to below as Cowley I, II and III.

In order to obtain a detailed description of the very complex structure of Fe_7S_8 we had to use both conventional 3D structure-determination techniques and refinement procedures, and in addition diffuse scattering measurements and analysis. It was only by feeding back into the refinements the more qualitative results obtained from the diffuse scattering (microtwinning and stacking faults) that a consistent structure emerged. One of the consequences of this unusual but very powerful approach is the length of this paper which is compiled in the following way: §2 describes the preliminary conventional structure determination; §3 introduces $4c$-type defects in the overall $3c$-type structure as revealed from diffuse scattering; §4 consists of a discussion of the resulting structure at that stage; §5 introduces the microtwinning mechanism in the form of stacking faults; §6 gives concluding remarks.

2. Average-structure determination

Fe_7S_8 powder was prepared from high-purity (5N) iron previously reduced in hydrogen at 1170 K and from distilled sulphur. The single crystals are grown by chlorine transport with a cold-zone temperature of about 923 K. Two points are to be noted:

under these conditions only hexagonal $2a$–$2a$–$3c$ Fe_7S_8 single crystals are obtained although the starting powder always belongs to the monoclinic modification $2a$–$2a$–$4c$ (it is impossible to get powders of the hexagonal form);

our crystals were grown at a temperature of about 923 K. This is lower than that for the crystals studied by Fleet (1971) or Nakano *et al.* (1979) who both used the solid-state reactions which required higher temperatures (~1170 K) than vapour transport.

Single-crystal X-ray diffraction patterns (Fig. 1) show the existence of the expected superstructure

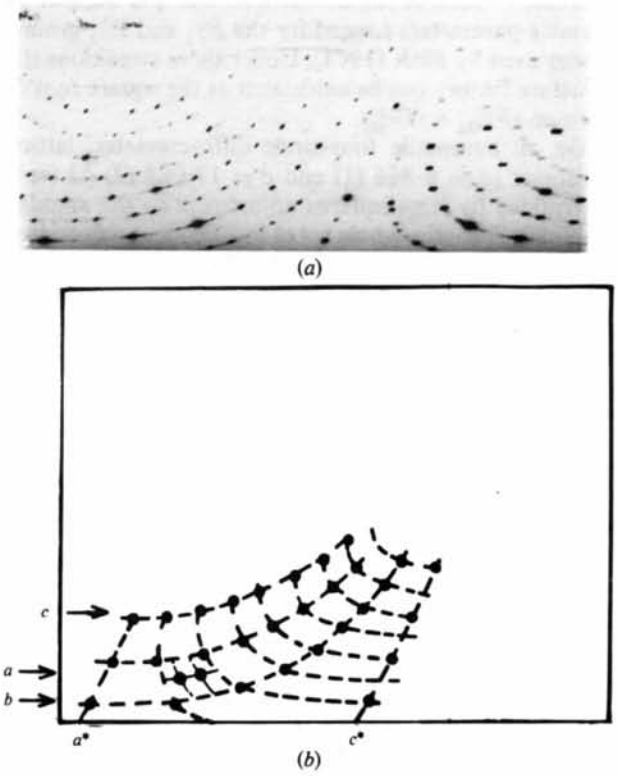

Fig. 1. (*a*) Diffraction pattern of the $h0l$ layer of $2a$–$2a$–$3c$ Fe_7S_8 (λ = Mo$K\alpha$, exposure time 7 d). (*b*) Indexing of the NiAs substructure reflections of (*a*). The complementary structure indexing is shown only on a small part of reciprocal space. The arrows indicate the rows along which the diffraction function is calculated. (*a*) 30l, (*b*) 20l, (*c*) 60l.

2a–2a–3c with superlattice reflections of relatively high intensity (much higher, for instance, than in $Ni_{17}S_{18}$). They also reveal diffuse streaks in the **c*** direction along the substructure rods as well as along the superstructure ones. Fig. 1 shows the *h*0*l* reciprocal layer of Fe_7S_8; this photograph obtained with monochromatic radiation from a doubly bent pyrolitic graphite monochromator is highly overexposed.

Under these conditions it is clearly seen that the systematic extinction rule found by the previous authors is strongly confirmed: the only authorized reflections on the 00*l* row obey the condition $l = 3n$. Again we find the same difficulty as for $Ni_{17}S_{18}$: the equality between the intensities $I_{hkl} = I_{khl} = I_{hk\bar{l}}$ and the systematic extinction suggests the hexagonal $P6_222$ space group for this compound (or the enantiomorphous $P6_422$). But in this group the equivalent positions *xyz* and $\bar{x}\bar{y}z$ are incompatible with the NiAs-type packing (*cf.* paper I). There is only one way to overcome this difficulty: to adopt a two-domain microtwinned model with, respectively, a 3_1 and a 3_2 axis, which is consistent with the extinction condition and with the iron and sulphur packing.

In fact, Nakano *et al.* (1979) have already shown that the $P3_121$ and $P3_221$ space groups give the best solution – same *R* factor but with half the number of variable parameters needed for the $P3_1$ and $P3_2$ groups earlier used by Fleet (1971). Under these conditions the structure factors can be calculated as the square root of the sum $|F|^2_{hkl} + |F|^2_{hk\bar{l}}$.

On an automatic four-circle diffractometer, lattice constants [$a = 6{\cdot}866$ (1) and $c = 17{\cdot}088$ (2) Å] were determined by least-squares adjustment to the angular readings. Then, the whole set of independent reflections, 573, was collected up to $2\theta = 65°$ (Mo $K\alpha$). The crystals of NiAs type prepared by vapour transport exhibit hexagonal platelet shapes and, when used for crystal structure determination, require a very careful absorption correction ($\mu = 140\ cm^{-1}$).

Table 1. *Positional and equivalent isotropic thermal parameters* (Å² × 10³) *in the* $P3_121$ *cell of* Fe_7S_8

$a = 6{\cdot}866$ (1), $c = 17{\cdot}088$ (2) Å. $B_{eq} = \frac{8}{3}\pi^2\Sigma_i\Sigma_j U_{ij} a_i^* a_j^* \mathbf{a}_i.\mathbf{a}_j$.

	Number per unit cell	*x*	*y*	*z*	B_{eq} (Å²)
Fe(1)	6	0·4718 (6)	0·4811 (6)	0·1583 (1)	2·2 (2)
Fe(2)	6	0·4985 (5)	0·4884 (6)	0·3309 (1)	2·4 (2)
Fe(3)	3	0·0289 (9)	0·000	0·83333	3·2 (2)
Fe(4)	3	0·4656 (6)	0·000	0·83333	2·8 (3)
Fe(5)	2·49 (3)	0·0205 (10)	0·000	0·33333	3·1 (3)
Fe(6)*	0·56 (3)	0·4521 (33)	0·000	0·33333	3·1 (3)*
S(1)	6	0·1610 (8)	0·3287 (10)	0·0744 (2)	2·5 (3)
S(2)	6	0·3356 (13)	0·1636 (9)	0·2472 (2)	1·7 (8)
S(3)	6	0·6688 (13)	0·3271 (11)	0·0847 (2)	2·1 (4)
S(4)	6	0·1623 (8)	0·8284 (9)	0·0885 (2)	1·7 (4)

* Constrained to the same U_{ij} values as Fe(5).

The refinement based on $F_{hkl} = (F^2_{hkl} + F^2_{hk\bar{l}})^{1/2}$, in which were introduced the positions previously given by Fleet (1971), using anisotropic temperature factors converged to $R = 12{\cdot}2\%$. At this stage two scale factors were introduced: one for the 52 substructure reflections and another for the 521 superstructure ones. A strong decrease was noted in the *R* factor which dropped to 7·05%, which is statistically highly significant, with a scale factor for the superstructure about 20% smaller than the substructure one. This indicates that in addition to the microtwin, there is another defect which disturbs the superstructure but does not affect the substructure. This is characteristic of a fault affecting the vacancy stacking without modification of the Ni and S sequences in the NiAs sublattice. Thus, with such a fault the coherence length for the substructure reflections must necessarily be larger than for the superstructure ones and the two types of reflections may not be treated with the same scale factors.

At this point we attempted systematic refinement of the occupation factors of the different iron sites including the vacant one. For the Fe(1) to Fe(4) sites (Table 1) the deviations from full occupancy were each time smaller than the standard deviation (0·01) and no modification of the *R* factor was noted. Thus these four

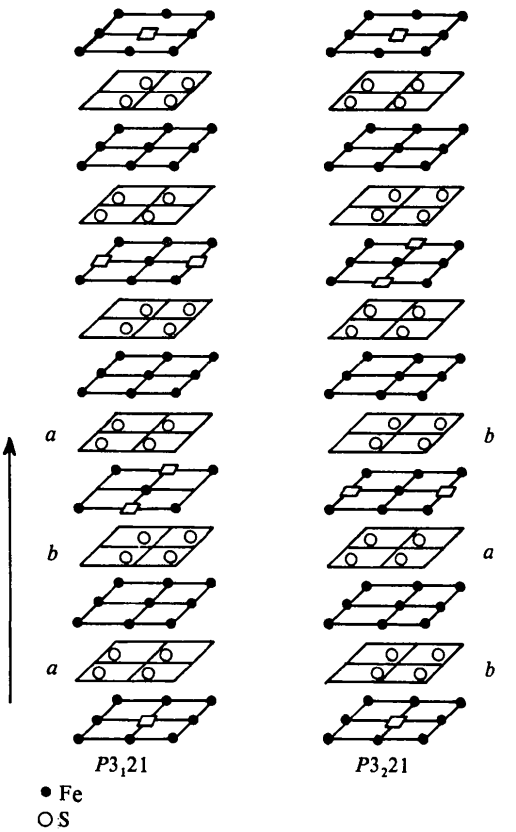

Fig. 2. Schematic representation of the vacancy ordering in the two domains of Fe_7S_8. The letters *a* and *b* refer to the types of sulphur plane as defined in §5.

sites can be considered as completely filled. On the other hand, the refinements on Fe(5) and Fe(6) occupation factors led to the values of Table 1 with about 20% vacancies on the 'filled' Fe(5) site and a quasi-perfect compensation (within the limit of standard deviations) for the 'vacant' Fe(6) site with a significant decrease of the R factor which reached the value of 4·72% for the whole set of independent reflections with a formula $Fe_{7\cdot003(8)}S$ which may then be considered as strictly Fe_7S_8. Schematic distributions of atoms and vacancies in the two types of domains are given in Fig. 2.*

3. Evidence for a 4c-type defect

As non-integral occupation factors have no physical meaning we tried to find an explanation for the observed incomplete occupancy of Fe(5) and for the presence of a fraction of iron atom on the Fe(6) site. It should be noted that neither Fleet (1971) nor Nakano *et al.* (1979) signaled this transfer from Fe(5) into Fe(6) sites and both describe a perfectly ordered structure.

In our case the fact that the sum of the Fe(5) plus Fe(6) occupation is equal to one atom per site suggests the nature of the defect. Indeed we have mentioned the existence of another form of Fe_7S_8, $2a$–$2a$–$4c$, for which the schematic packing is indicated in Fig. 3(*c*). In both cases $3c$ and $4c$, between two Fe planes with vacancies, there are two sulphur planes surrounding a non-vacant Fe plane (as in Fig. 2) which are not represented in Figs. 3(*a*), 3(*b*) and 3(*c*). In this $4c$ modification there are four (instead of three for the $3c$ modification) different kinds of Fe planes with vacancies, among which three are identical with the $3c$ hexagonal ones (vacancies with $x,y \simeq \frac{11}{22}, \frac{1}{2}0$, and $0\frac{1}{2}$), while in the fourth the vacancies are situated on the $xy = 00$ chain (on $z = \frac{1}{2}$), which is never perturbed by vacancies in the ideal trigonal packing (Fig. 3*a*). It is on this 00 chain that partial vacancies are found – on the Fe(5) site, Fig. 3(*b*) – in our refinement indicating the occurrence of this forbidden kind of Fe plane with vacancies in the $3c$ packing. The inclusion of such planes with empty Fe(5) sites decreases the average occupancy of Fe(5) with a strictly complementary increase of the Fe(6) site occupancy in order to keep the Fe_7S_8 composition. This defect is only a fault for the superstructure but does not affect the substructure: it corresponds to another distribution of vacancies over the iron sites and then is not detectable on the main lattice reflections which only take into account the changes in stoichiometry.

Moreover, the intensity lost on the superstructure reflections as a consequence of this disorder should reveal itself according to the correlation existing between the planes of empty Fe(5) sites. If such planes were uncorrelated with each other, continuous diffuse streaks should be observed (planar disorder) along the **c*** direction including the $h - k = 6n$ ones where the stacking fault does not contribute (see below). This is not observed, but instead one finds weak diffuse maxima along the $00l$ direction for $l = 3n/2$ of the $3c$ cell (Fig. 4). On the other rods parallel to **c***, these weak maxima are either masked by the strong streaks resulting from the stacking fault or too weak to be observed because of being too far in reciprocal space (for $60l$ for instance). These broad and diffuse maxima show that short-range order exists for the Fe planes with empty Fe(5) sites [and filled Fe(6) sites]. Their localization in reciprocal space corresponds to the $00l$, $l = 2n$ reflections of the $4c$ modification of Fe_7S_8 (the

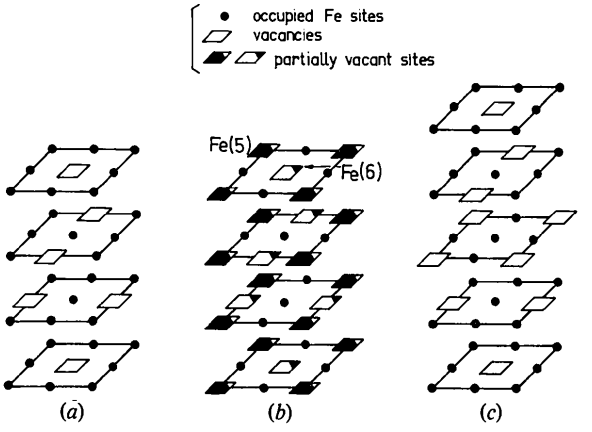

Fig. 3. Schematic representation of vacancy localization in Fe_7S_8. Only the iron planes with vacancies are represented. Between each of these planes there is one filled iron plane surrounded by two sulphur planes. (*a*) Ideal $3c$. (*b*) Computed solution for $3c$. (*c*) Ideal $4c$.

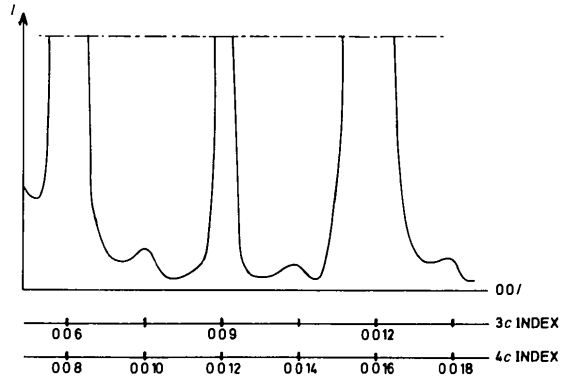

Fig. 4. Diffraction observed along the $00l$ row with $3c$ and $4c$ indexing showing the occurrence of weak reflections of $4c$ type.

* Lists of structure factors and anisotropic thermal parameters have been deposited with the British Library Lending Division as Supplementary Publication No. SUP 38250 (6 pp.). Copies may be obtained through The Executive Secretary, International Union of Crystallography, 5 Abbey Square, Chester CH1 2HU, England.

only ones authorized) which are not confused with the 3c-type reflections (Fig. 4). This strongly indicates the occurrence of 4c sequences in the crystal with a coherence length deduced from the width of the difusion maxima of about 50 Å corresponding to sequences of about two 4c cells which are included in the overall 3c-type Fe_7S_8.

A quantitative confirmation of such defects can be given if their effect on the structure determination is reanalysed:

the substructures of the 3c and 4c cells always coincide because they correspond to the NiAs sublattice which is common to the two supercells;

on the other hand, the superstructure reflections generally do not coincide because the intervals between two substructure reflections are divided either by three or by four following the kind of supercell;

this is not true for the superstructure reflections with $l = 3n$ in the 3c lattice which are localized on the reciprocal-space points of the $l' = 4n$ of the 4c lattice: for instance, this is the case of the $00l$ with $l = 9$ and 15 corresponding to $l' = 12$ and 20 of the 4c lattice in Fig. 4. For these reflections the same coherence as for the substructure reflections must be expected for the same reason.

Indeed, if these reflections with $l = 3n$ are computed with the same scale factor as the substructure the R factor decreases from 4·72 to 4·25% with exactly the same number of variable parameters. This is a quantitative demonstration of the full coherence of the two types of superstructures for this special kind of reflection. This also strongly confirms our hypothesis of a new defect corresponding to the occurrence of 4c sequences in addition to the microtwin. This result, on the other hand, is in excellent agreement with the Mössbauer work of Ovanesyan, Trukhtanov, Odinets & Novokov (1971) who also found the inclusion of about 20% of the 4c phase in the 3c hexagonal pyrrhotite.

The final R factor of 4·25% corresponds to a partial R equal to 2·4% for the 52 substructure reflections and a partial R equal to 5·5% for the 521 superstructure reflections including those of zero intensity, which is a homogeneous and satisfactory result.

4. Discussion and atomic correlations

As mentioned earlier, the previous structural determination did not reveal any disorder in the vacancy stacking in contrast with our results. This is only an apparent contradiction because our crystals were prepared at lower temperature than the ones used by either Fleet (1971) or Nakano *et al.* (1979). Since the 4c type of Fe_7S_8 is more stable at low temperature, it is not completely surprising to encounter it in our preparation, whereas the crystals grown at higher temperatures are free from it. Unfortunately, attempts to grow single crystals by vapour transport at higher temperatures, in order to verify this interpretation, were unsuccessful.

In other respects our R factor and our atomic coordinates are close to the ones published in the recent re-examination of the 3c-Fe_7S_8 structure by Nakano *et al.* (1979). This indicates that low-temperature-grown single crystals of Fe_7S_8 while less stable are only slightly modified in their relative atomic disposition.

Concerning the structure description, one finds in this compound the characteristics of the NiAs-type iron sulphides, which is to exhibit in-plane iron–iron distances very different from the ideal ones. Such distances are obtained from the NiAs-type cell with lattice constants of the subcell: space group $P6_3/mmc$, $a = 3{\cdot}433$, $c = 5{\cdot}696$ Å with two Fe on 000 and $00\frac{1}{2}$ and two S on $\frac{1}{3}\frac{2}{3}\frac{1}{4}$ and $\frac{2}{3}\frac{1}{3}\frac{3}{4}$.

The effect of the vacancies is to perturb three of the four iron chains in the **c** direction, with a very strong displacement of the Fe(1) toward the Fe□ vacant site and a corresponding relaxation of the other Fe–Fe distances (Fig. 5*a*). The average Fe–Fe distances along these chains [including the Fe(1)–Fe□ distances] of 2·87 Å are close to that observed along the unperturbed

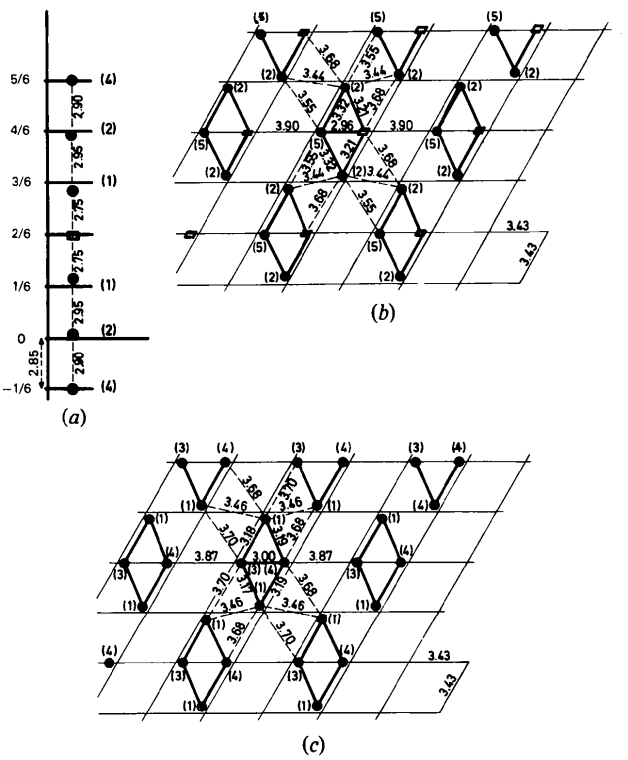

Fig. 5. The numbers within brackets refer to the Fe atoms as defined in Table 1. (*a*) Fe–Fe correlation along **c** for the iron chains with vacancies. (*b*) Fe–Fe correlations within the planes with vacancies. The represented plane is at $z = \frac{1}{3}$. (*c*) Fe–Fe correlations in the planes without vacancies. The represented plane is at $z = \frac{5}{6}$.

chain; the Fe(3)–Fe(5) distance is 2·86 Å. Both distances are a little larger than the ideal value by reason of the x, y component of the atomic displacements.

The vacancies also introduced a difference between the two independent types of iron planes. In the plane which does not contain vacant sites one finds a 'lozenge correlation' with very short distances compared with the ideal value of 3·43 Å. On the other hand, the introduction of a vacancy at the lozenge corner in the second kind of Fe plane relaxes the true Fe–Fe distances which become appreciably larger (Figs. 5*b* and 5*c*).

Finally, the normal Fe atoms [Fe(1) to Fe(5)] are in distorted sulphur octahedra with average distances ranging between 2·44 and 2·45 Å, that is to say close to the ideal value of 2·44 Å. The relaxation is weak around the vacancy [taken on the Fe(6) position] with an average value of 2·46 Å.

5. Stacking faults

Exactly as done before for $Ni_{17}S_{18}$ (paper I), the question is now to define the microtwinning mechanism. For exactly the same reasons we conclude here again that the occurrence of stacking faults is needed in order to explain the change, around an Fe plane with vacancies, of a sulphur a-type plane at $z + \frac{1}{12}$ and a sulphur b-type plane at $z - \frac{1}{12}$ for the first kind of domain ($P3_121$) to a sulphur b-type plane at $z + \frac{1}{12}$ and a sulphur a-type plane at $z - \frac{1}{12}$ for the second kind of domain ($P3_221$) (Fig. 2).

On the photograph of Fig. 1, it can be seen that streaks are present in the $\mathbf{c}^*$ direction along all the superstructure rows as well as along some substructure ones confirming the existence of stacking defects. On the other hand, in the hexagonal plane, the reflections and streaks are very sharp, indicating a large in-layer correlation length.

The systematic distribution of the streaking is the same as previously observed with $Ni_{17}S_{18}$. Indeed, in substructure notation, the substructure reflections with $h - k = 3n$ do not exhibit any broadening, even the strongest ones, while for those with $h - k \neq 3n$ the broadening is visible far into reciprocal space.

This indicates the occurrence of a fault which affects the main reference NiAs lattice and which is the same as the one discussed for $Ni_{17}S_{18}$ in paper I; that is to say, a translation vector with components $\mathbf{S} = \pm(\mathbf{a} - \mathbf{b})/3$ which interchanges the sixfold and threefold axis of the hexagonal sublattice. As a matter of fact only this kind of defect can explain the different widths observed in the substructure; it introduces, indeed, in the diffraction function

$$I/N = \sum_m \sum_n |\overline{F_n^* F_{n+m}}| \exp(2\pi i \mathbf{u}.\mathbf{R})$$

a phase factor $\exp(\pm 2\pi i \mathbf{u}.\mathbf{S})$ which not only keeps the full coherence for the $h - k = 3n$ rows but also shifts the phases of the $h - k \neq 3n$ rows relative to one another destroying their ideal coherence. This fault (Fig. 6) results in a sulphur plane which is a type for the Fe plane just before the fault being also of b type for the Fe plane after the fault, and in consequence allows the change from one kind of domain of the microtwin to the other.

As for $Ni_{17}S_{18}$, the systematic distribution of the streaking enables us to eliminate the two other possible mechanisms of the microtwinning.

(i) To have two superposed sulphur planes of the same type, because in this case the streaking would only depend on the l index (*cf.* paper I), which is inconsistent with the observations.

(ii) To have errors in the vacancy stacking which would not produce substructure streaking because it does not introduce any modification of the sublattice stacking ($\mathbf{S} = 0$). In addition, this kind of fault is not compatible with the ferrimagnetic behaviour of this material. Indeed, since the spins in the NiAs-type structure are alternately up and down in the **c** direction, the ferrimagnetism necessarily supposes vacancies strictly disposed every two iron planes. A fault in vacancy stacking which would introduce odd intervals between vacant sites in the **c** direction would destroy the ferrimagnetism.

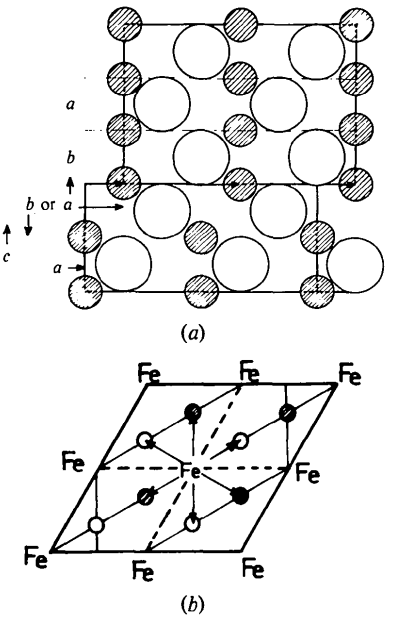

Fig. 6. The stacking fault in Fe_7S_8. (*a*) In the (110) plane of the direct lattice. The translation (**a** **b**)/3 (substructure notation) induces the $a \rightleftharpoons b$ transformation and the change from one domain to the other. a and b refer to sulphur-plane types as defined in § 5. (*b*) The fault vector in the hexagonal plane of Fe_7S_8.

Consequently, the only mechanism consistent with the experimental results is the glide vector $(\mathbf{a}-\mathbf{b})/3$ of Fig. 6 which explains the domain change at the fault and accounts for the observed diffuse streaks. The discussion of the defect has been given in detail in paper I and we will not repeat it here. We need only recall that there is no change in the Fe coordination, that the sixfold sulphur coordination is changed from trigonal prismatic to octahedral and that along the **c** direction the iron and sulphur chains are interchanged.

Concerning the fault-rate determination, the substructure approximation used for $Ni_{17}S_{18}$ is no longer valid here:

in Fe_7S_8, the superstructure reflections are strong owing to the higher amount of vacancies and to the larger atomic displacements with respect to the ideal NiAs position;

in Fe_7S_8, the fault rate is high enough to produce diffuse scattering, not only around the strongest substructure reflections but also along the superstructure rows.

The two fault vectors in the substructure (*cf.* paper I) turn into six possible translations in the superstructure cell (Fig. 6) with fault rates $\alpha(1\rightarrow 2)=\alpha(2\rightarrow 1)=\alpha$. Following Cowley's equation (9) (Cowley I), we write

$$I/N=\sum_i g_i \frac{F_i^*}{1-(1-A_i)\exp[2\pi i\mathbf{u}.\mathbf{R}_i]} \times\left\{F_i+\frac{\sum_j \alpha_{ij}\exp[2\pi i\mathbf{u}.\mathbf{R}_i+S_{ij}]}{1-(1-A_j)\exp[2\pi i\mathbf{u}.\mathbf{R}_j]} \times[F_j+\cdots]\right\}+\text{c.c.}-\sum_i g_i|F_i|^2, \quad (1)$$

where $A_i=A_j=A_k=\cdots=6\alpha$, $R_1=R_2=R$, $g_1=g_2=\frac{1}{2}$.

Therefore

$$2I/N=\sum_{i=1}^{2}\frac{F_i^*}{1-(1-6\alpha)\exp[2\pi i\mathbf{u}.\mathbf{R}]} \times\left(F_i+\frac{\alpha\exp[2\pi i\mathbf{u}.\mathbf{R}]\sum\cos}{1-(1-6\alpha)\exp[2\pi i\mathbf{u}.\mathbf{R}]} \times\left\{F_j+\frac{\alpha\exp[2\pi i\mathbf{u}.\mathbf{R}]\sum\cos}{1-(1-6\alpha)\exp[2\pi i\mathbf{u}.\mathbf{R}]} \times[F_i+\cdots]\right\}\right)+\text{c.c.}-\sum_{i=1}^{2}|F_i|^2. \quad (2)$$

The shift contribution $\sum\cos$ is

$$\sum\cos=\tfrac{2}{3}[\cos 2\pi(h-k)/6+\cos 2\pi(2h-k)/6+\cos 2\pi(h+2k)/6] \times(1+\cos 2\pi l/3+\cos 2\pi 2l/3) \quad (3)$$

in which the last bracket takes into account the shifts of the origin in the **c** direction at the fault.

We have solved (2). The solution is

$$\begin{aligned}2I/N=\Big[&(|F_1|^2+|F_2|^2)\\&\times\{1+2\cos(2\pi\mathbf{u}.\mathbf{R})(1-6\alpha)\\&\times[(1-6\alpha)^2-(\alpha\textstyle\sum\cos)-1]\\&-[(1-6\alpha)^2-(\alpha\textstyle\sum\cos)^2]^2\}\\&+(F_1^*F_2+F_1F_2^*)\{2\cos(2\pi\mathbf{u}.\mathbf{R})\\&\times\alpha[(1-6\alpha)^2-(\alpha\textstyle\sum\cos)^2+1]\\&-4\alpha\textstyle\sum\cos(1-6\alpha)\}\Big]\\&\times\{1-4\cos(2\pi\mathbf{u}.\mathbf{R})(1-6\alpha)\\&\times[(1-6\alpha)^2-(\alpha\textstyle\sum\cos)^2+1]\\&+2\cos(2\pi\mathbf{u}.2\mathbf{R})[(1-6\alpha)^2-(\alpha\textstyle\sum\cos)^2]\\&+4(1-6\alpha)^2+[(1-6\alpha)^2-(\alpha\textstyle\sum\cos)^2]^2\}^{-1}.\end{aligned} \quad (4)$$

For the substructure reflections not influenced by the stacking fault (*i.e.* indices with $h-k=6n$, $l=6$), one gets $F_1=-F_2$. In this case $\sum\cos=6$ and $I/N\rightarrow|F|^2\times(1-6\alpha)/6\alpha$ when $\cos\{2\pi\mathbf{u}.\mathbf{R}\}\rightarrow 1$ which is a confirmation of the validity of (4) and again confirms the efficiency of Cowley's theory. For the strongest superstructure reflections, with $l\neq 3n$, $\sum\cos=0$, the coherence terms $F_1^*F_2+F_1F_2^*$ are zero and only remain the twin terms with $I/N=(|F_1|^2+|F_2|^2)(1-3\alpha)/3\alpha$. The coherence terms are different from zero for all the other reflections but it is known that integration by the diffractometer (Cowley III) leads to data which can be computed in a microtwinned model.

The fault rate is determined by adjusting the graph computed with (4) to the observed intensities. The best result is obtained for an α value equal to 0·03. As is normal in these conditions, although the agreement is excellent for the streaks, the calculated peaks at the Bragg points are sharper than the observed ones. This can be explained by the fact that in (4) we have not introduced any crystal form factor or resolution correction. The complete diffraction function must be the result of the convolution of (4) with the experimental resolution functions which include crystal size, sample mosaic, monochromator mosaic, beam divergence, *etc.* If all these corrections are approximated by a slit function corresponding to the observed crystal size on the photograph the equation becomes

$$I(l)_{\text{(calculated)}}=\int_{-a/2}^{-a/2} I/N(l')\mathrm{d}l', \quad (5)$$

in which the integration is performed with respect to the l index in reciprocal space (along the streaks). The numerical integration gives a correct broadness for the peaks when a is taken as 0·3 l units in superstructure

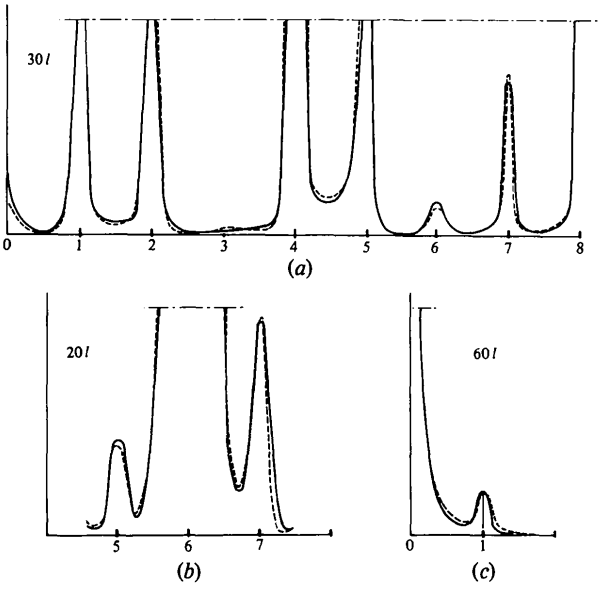

Fig. 7. Diffraction function observed (full lines) and calculated (dashed lines) for (*a*) a superstructure row, (*b*) a broadened substructure row and (*c*) a non-perturbed substructure reflection. Lorentz polarization corrections were made but no absorption correction was taken into account.

notation. In any case this does not modify the α value because it was determined from the streaks between Bragg reflections in regions where (4) only varies very smoothly and is not sensitive to the integration effect. The results are graphically shown in Fig. 7.

6. Conclusion

We have shown that the microtwin observed in 3*c*-type Fe_7S_8 crystals can be simply explained by a planar fault of the same type as the one encountered in hexagonal close packing which exchanges the different threefold axis and modifies, at the fault, the fundamental stacking of the NiAs-type structure.

Let us point out further that this fault is present in all the 3*c*-type Fe_7S_8 crystals we have examined, and moreover with about the same fault rate. It is also present, in addition to $Ni_{17}S_{18}$, in the few crystals of monoclinic 4*c*-type Fe_7S_8 we obtained by vapour transport. But the problem is complicated in the latter case by an additional macrotwinning due to the monoclinic deformation ($\gamma = \pm 89{\cdot}63°$). The Bragg peaks from each of these domains are generally separated and in each domain a microtwinning with diffuse streaks almost identical to the ones of 3*c*-type Fe_7S_8 is observed.

It is noted that in the Fe–S phase diagram the kind of planar fault described above is specific for compositions close to Fe_7S_8 and that it disappears when the iron content increases and then gives rise to other faults which do not perturb the average lattice.

References

BERTAUT, E. F. (1953). *Acta Cryst.* **6**, 557–561.

COLLIN, G., CHAVANT, C. & COMÈS, R., (1983). *Acta Cryst.* B**39**, 289–296.

COWLEY, J. M. (1976*a*). *Acta Cryst.* A**32**, 83–87.

COWLEY, J. M. (1976*b*). *Acta Cryst.* A**32**, 88–91.

COWLEY, J. M. & AU, A. Y. (1978). *Acta Cryst.* A**34**, 738–743.

FLEET, M. E. (1971). *Acta Cryst.* B**27**, 1864–1867.

MUKHERJEE, B. (1969). *Acta Cryst.* B**25**, 673–676.

NAKANO, A., TOKONAMI, M. & MORIMOTO, N. (1979). *Acta Cryst.* B**35**, 722–724.

NAKAZAWA, H., MORIMOTO, M. & WATANABE, E. (1975). *Am. Mineral.* **60**, 359–366.

OVANESYAN, N. S., TRUKHTANOV, V. A., ODINETS, G. Y. & NOVOKOV, G. V. (1971). *Sov. Phys. JETP*, **33**, 1193–1197.

TOKONAMI, M., NISHIGUSHI, K. & MORIMOTO, N. (1972). *Am. Mineral.* **57**, 1066–1068.

VAN LANDUYT, J. & AMELINCKX, S. (1972). *Mater. Res. Bull.* **7**, 71–80.

Acta Cryst. (1983). B**39**, 303–306

Bonding in Lithium Tetrafluoroberyllate(II)

BY D. M. COLLINS, M. C. MAHAR AND F. W. WHITEHURST

Department of Chemistry, Texas A&M University, College Station, Texas 77843, *USA*

(*Received* 8 *June* 1982; *accepted* 10 *December* 1982)

Abstract

The electron deformation density of Li_2BeF_4 has been investigated with regard to the bonding description of McGinnety [*J. Chem. Phys.* (1972), **59**, 3442–3443]. Data in the range $0 < \sin\theta/\lambda \leq 1{\cdot}20$ Å^{-1} were obtained in a single-crystal X-ray diffraction experiment ($R = 0{\cdot}021$ for 984 unique reflections) and used to represent the deformation density in *X*–*X* maps. The results conform to the expected covalent character associated with Be–F bonds but offer no support for the proposed Li–F covalent bonding.

0108-7681/83/030303-04$01.50 © 1983 International Union of Crystallography